3

Schieber, Juergen, Remus Lazar, Kevin Bohacs, Bob Klimentidis, Mirela Dumitrescu, and Jeff Ottmann, 2016, An SEM study of porosity in the Eagle Ford Shale of Texas— Pore types and porosity distribution in a depositional and sequence-stratigraphic context, *in* J. A. Breyer, ed., The Eagle Ford Shale: A renaissance in U.S. oil production: AAPG Memoir 110, p. 167–186.

An SEM Study of Porosity in the Eagle Ford Shale of Texas—Pore Types and Porosity Distribution in a Depositional and Sequence-stratigraphic Context

Juergen Schieber

Department of Geological Sciences, Indiana University, 1001 E 10th St., Bloomington, Indiana 47405, U.S.A. (e-mail: jschiebe@indiana.edu)

Remus Lazar, Kevin Bohacs, Robert Klimentidis, Mirela Dumitrescu, and Jeff Ottmann

ExxonMobil Upstream Research Company, 22777 Springswood Village Pkwy., Spring, Texas 77389, U.S.A. (e-mails: ovidiu.remus.lazar@exxonmobil.com; kevin.m.bohacs@exxonmobil.com; crymkli@aol.com; mirela.dumitrescu@exxonmobil.com; jeff.ottmann@exxonmobil.com)

ABSTRACT

Although typically considered with a focus on high-resolution petrography, shale porosity should not be thought of as a stand-alone petrographic feature. Shale and mudstone porosity is the outcome of a long succession of processes and events that span the continuum from deposition through burial, compaction, and late diagenesis. For the Eagle Ford Shale this journey began with accumulation in intra-shelf basins at relatively low latitudes on a southeast-facing margin during early parts of the late Cretaceous. To understand the factors that generated and preserved porosity in this economically important interval, a scanning electron microscope study on ion-milled drill-core samples from southern Texas was conducted to understand the development of petrographic features and porosity and place them in stratigraphic context.

The studied samples show multiple pore types, including pores defined by mineral frameworks (clay and calcite), shelter pores in foraminifer tests and other hollow fossil debris, and pores in organic material (OM). In many instances, framework and shelter pores are filled with OM that has developed pores due to maturation. Large bubble pores in OM suggest that hydrocarbon liquids were left behind in or migrated into these rocks following petroleum generation and that the bubbles developed as these rocks experienced additional thermal stress. These larger OM pores indicate deeper seated interconnection on ion-milled surfaces and in three-dimensional image stacks.

DOI:10.1306/13541961M1103589

The largest pores occur in the infills of foraminifer tests. The framework of crushed carbonate debris in planktonic fecal pellets shows intermediate levels of porosity, and the silicate-rich matrix that encloses framework components has the smallest average porosity.

The distribution of pore types is not uniform. Our hypothesis is that facies association is an important factor that determines bulk porosity and influences reservoir performance. The observed variability in the attributes of the described distal, medial, and proximal facies associations is thought to translate into significant variability of rock properties such as total organic carbon and porosity. In turn, this variability should control the quality and distribution of the intervals that are optimum sources and reservoirs of hydrocarbons in the Eagle Ford Shale. The medial facies association most likely has the best porosity development when a favorable combination of more commonly abundant calcareous fecal pellets and organic material versus clay content is present. The systematic arrangement of facies associations into parasequences provides the basis for testing and predicting the best development of optimal reservoir facies within a sequence-stratigraphic framework in the Eagle Ford Shale.

INTRODUCTION

Mudstones are inherently heterogeneous, composed of multiple component grains, at variable proportions, with a potentially wide range of properties. Thus, predicting key properties such as rock strength, porosity, and permeability from well-log readings and general lithologic assessments tends to be rather difficult. On the other hand, detailed description of mudstone successions within a sequence-stratigraphic framework allows us to organize sedimentary facies, to predict lateral distribution, and to extract order from seeming chaos (Lazar et al., 2013, 2015).

In recent years the Cretaceous Eagle Ford Shale has been one of the most actively drilled hydrocarbon deposits in the United States, and in 2013 alone (data provided by the Railroad Commission of Texas), it produced 3.7 million cubic feet of gas and 0.7 million barrels of oil per day. With proven reserves in excess of 1 billion barrels of oil and 8 trillion cubic feet of gas (U.S. EIA data) it qualifies as a giant oil and gas field (Halbouty et al., 1970) and its output has been crucial to the growth in Texas oil and gas production in recent years.

The presented observations are based on work conducted in the 2009–2011 time frame and were initially presented at the 2012 AAPG meeting in Long Beach (Schieber et al., 2012). Since then several other publications on Eagle Ford porosity using ion-milled samples have been released (Driskill et al., 2013; Jennings and Antia, 2013; Rine et al., 2013), and we have therefore chosen to present a perspective where porosity development is placed in the context of depositional parameters and history.

With examples from the lower portions of the Cretaceous Eagle Ford Shale of southwest Texas, we aim to show how integration of core descriptions, petrographic thin sections, and high-resolution electron microscopy gives us an understanding of the factors that control the distribution of porosity and reservoir quality at the parasequence scale. We propose that this type of analysis is a fundamental as well as efficient step in the process of developing predictive stratigraphic models for the Eagle Ford Shale and also is of general applicability in the search for unconventional oil and gas resources in fine-grained sedimentary rocks.

EAGLE FORD SHALE BOUNDARY CONDITIONS

The Cenomanian–Turonian time interval was characterized by a greenhouse climate, rising sea level, and continued continental dispersion with the opening of the South Atlantic and the closing of the Tethys Ocean (e.g., Salvador, 1987; Goldhammer and Johnson, 2001; Bohacs et al., 2012). Primary "soft part" organic matter producers included cyanobacteria and chlorophytae, whereas "hard part" producers (calcareous and siliceous) included coccolithophores, foraminifera, and radiolaria (e.g., Bostick, 1960; Lundquist, 2000; Bohacs et al., 2011).

The studied area was located in the southern Western Interior Seaway on continental crust, on the edge of the expanding Gulf of Mexico oceanic basin (Figure 1; e.g., Salvador, 1987; Adams and Carr, 2010; Bohacs et al., 2011; Bohacs et al., 2012). During the Cenomanian–Turonian the Eagle Ford Shale accumulated at subtropical paleolatitudes on a storm-wave-dominated shelf, within a series of mid- to outer-shelf basins that were regionally isolated from major siliciclastic influx (e.g., Powell, 1965; Trevino, 1988; Miller, 1990; Dawson and Almon, 2010; Donovan and Staerker, 2010; Bohacs et al., 2011; Hentz and Ruppel, 2011; Bohacs et al., 2012; Bryer et al., 2013). Shelfal basins were subject to tropical cyclones in a dry to very dry climate. Sea water was persistently warm with annual average sea surface temperatures ranging from 25 to 29°C, which is favorable for high primary carbonate production and low destruction under a

Figure 1. Geological setting for the Eagle Ford Shale. Location of study area is marked with black oval (after Bohacs et al., 2011). 200 km (124.3 mi)

water column that was sluggish, saline, and prone to stratification (e.g., Bohacs et al., 2011, 2012).

Physical, biogenic, and chemical data indicate that the Eagle Ford Shale accumulated in depositional subenvironments that were characterized by significant variations in primary biogenic production, bottom-energy and oxygen levels, as well as sediment accumulation modes and rates. Sediment was delivered as organo-mineralic aggregates (Syvitski, 1991), fecal pellets, and floccules by traction transport (Schieber et al., 2007), sediment gravity flows, and suspension settling (benthic and pelagic). Benthic energy levels were commonly capable of transporting sand-sized grains as evidenced by a variety of physical sedimentary structures including scour surfaces, wave, current, and combined-flow ripples, graded beds, fossil and pyrite lags, and potentially wave-enhanced sediment-gravity-flow beds (Macquaker et al., 2010; Bohacs et al., 2011). Paleoredox conditions in the bottom waters were frequently dysoxic with the potential for intermittent anoxic and oxic intervals. Redox conditions were interpreted based on the presence of *in situ* body fossils including benthic foraminifera as well as articulated epibenthic and shallow-burrowing bivalves that indicate significant and recurring periods of benthic oxygenation. The epi- and endobionts show low diversity (~2–3 genera) and are of a type especially adapted for life on a soft and water-rich substrate (soupground) under persistently dysoxic conditions (e.g., *Pectinidae*, *Pteriidae*, *Inoceramidae*; Brett and Allison, 1998; Bohacs et al., 2011). Their size distribution and growth-ring count are relatively narrow, suggesting colonization events that were episodic. These biota co-occur with ichnofossils and sedimentary structures that indicate increased benthic oxygen and energy levels, although the thin-walled and articulated nature of the macrofossils indicates minimal transport. Ichnogenera include "mantle-and-swirl" (sediment-swimmer) traces (Lobza and Schieber, 1999), *Planolites*, *Chondrites*, *Helminthopsis*, *Palaeophycus*, *Phycosiphon*, and sparse *Zoophycos* (Bohacs et al., 2011). These ichnotaxa are present in commonly recurring facies associations (discussed later).

Pelagic body fossils are quite common, comprising mostly pellets and aggregates of coccoliths, as well as isolated coccolith plates, calcareous foraminifera, calcispheres, and sparse radiolaria (e.g., Bostick, 1960; Lundquist, 2000). The carbonate allochems all show various degrees of transport and reworking, suggesting that they formed *in situ*. The calcareous allochems appear to be an important component of porosity development and distribution, with significant pores preserved between and within them.

Mudstone character and distribution were influenced at the local scale by evolving paleobathymetry that was influenced by the development of benthic carbonate bioherm complexes, salt movement, and syndepositional faulting (Bohacs et al., 2011). The Eagle Ford Shale has been interpreted to be a

transgressive and highstand sequence set with significant onlap at the base and variable truncation at the top (Donovan and Staerker, 2010; Bohacs et al., 2011).

METHODS

Core Description

Eagle Ford Shale cores taken from wells drilled in the Maverick Basin of south Texas (LaSalle and Dimmitt Counties) were examined at the millimeter scale using a standard protocol for determining texture, bedding, composition, and bioturbation index (Table 1), as well as type and abundance of physical sedimentary structures and body and trace fossils, type, habit, and distribution of nodules, and color (e.g., Bohacs, 1990; Lazar et al., 2014). The cores penetrated mudstones of the Lower Eagle Ford Group as defined by Donovan and Staerker (2010). Facies examination revealed significant variability in the relative abundance of each physical, biological, and chemical attribute at lamina to bed to bedset scale recorded in repeated facies associations (FAs). The observed and recorded features are summarized in Figure 2, which also serves as the legend for the FA summaries (Figures 3–5). FAs are interpreted as the outcome of mud accumulation under a variety of depositional conditions with significant variations in primary biogenic production, bottom-energy and oxygen levels, sediment accumulation modes and rates, on the distal, middle, and proximal portions of a storm-wave-dominated shelf. We aggregated facies associations with distinct vertical stacking patterns into facies association successions (FASs), compared them among all our examples, and summarized them in Figures 3 through 5. We interpreted FASs to represent parasequences (Bohacs, 1998; Bohacs et al., 2014).

Ion Milling and SEM

The porosity observations presented here draw on a representative suite of 20 samples that were collected from all facies associations during core description. The Eagle Ford samples range in maturity from about 1.2 to 1.5 % R_o (gas maturity window). Subsamples of up to 10 x 10 mm size were cut from these samples, in an orientation perpendicular to bedding and marked precisely on preprocessing photos of samples. Samples were mounted on custom made 1/2 inch diameter sample holders and ion milled over the entire exposed area (25–100 mm^2 depending on sample geometry). These sample holders were designed to fit a maximum

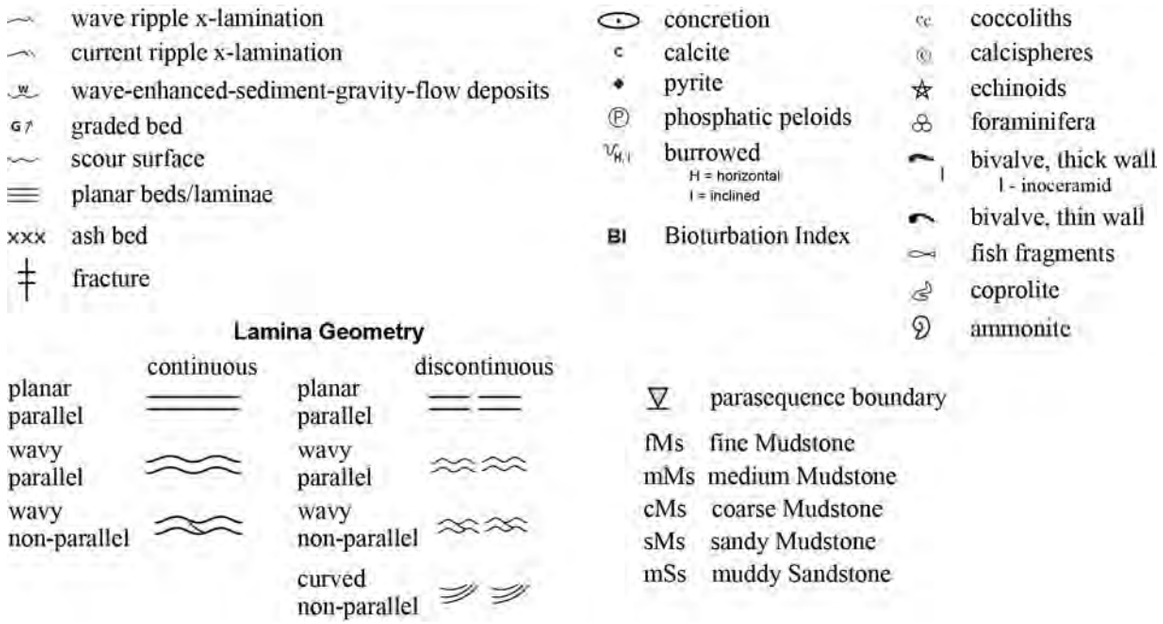

Figure 2. Observed and recorded sedimentary features in the Eagle Ford Shale. This figure is also the legend for Figures 3–5.

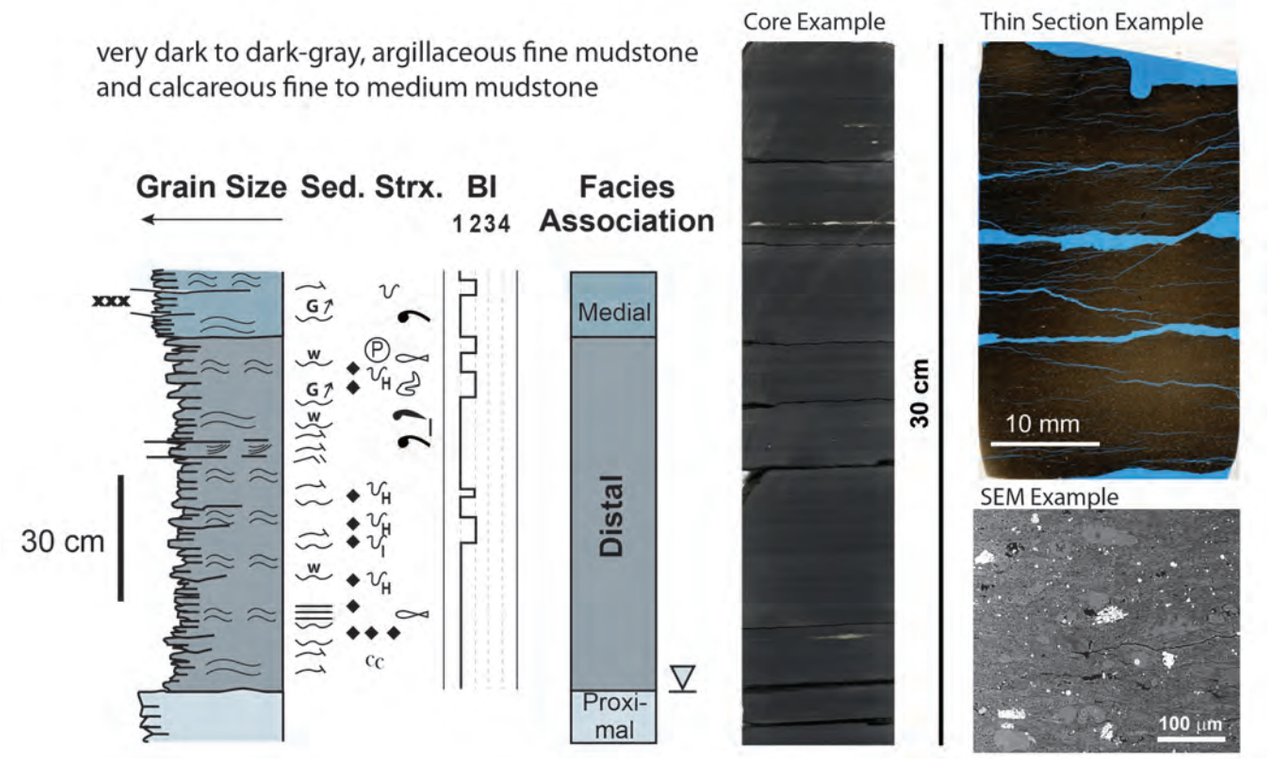

Figure 3. Overview of the distal facies association (FA-D). At left, a summary of sedimentary features observed in the FA-D (see Figure 2 for legend). In the middle, a typical example of FA-D in drill core. Original laminae are preserved to various degrees following bioturbation. At right, photomicrographs of FA-D in a thin section and an ion-milled sample (bottom). Notice the suspension of larger and denser grains in a finer matrix in the SEM image. The grains include mollusk fragments, scattered fish scales, and pyritized fish bones as well as scattered foraminifera, calcispheres, and sparse to common fecal pellets. Foraminifer tests are mostly filled with calcite spar (~90%), authigenic clays, and organic material. Foraminifera are scattered through a groundmass that consists of compressed calcareous fecal pellets (~20–30% planktonic) and a mixture of clays, quartz silt, calcareous debris, volcanic ash components, and organic material.

diameter sample into a Gatan 600 DuoMill™, an ion mill originally designed for preparation of TEM specimens, but now rebuilt for the milling of large diameter (1/2") samples (Schieber, 2010, 2013). The Gatan 600 DuoMill™ has a broadly focused argon ion beam under which the sample rotates. This results in a rather gentle polishing action and produces a smooth to gently undulose surface.

The possibility that artificial pores might be produced in organic material-rich areas due to ion beam heating was a serious concern. We adopted the following procedure to eliminate misinterpretation of artifacts. First, samples were given a multistep low-pressure mechanical polish to 0.1 µm, rinsed and cleansed gently with distilled water, blow-dried with compressed air, and then examined and photographed under SEM. Second, after first-pass ion milling with a GATAN 600 DuoMill™, samples were examined again under SEM, and the same areas as previously were examined and photographed a second time. Third, photographs of mechanically polished versus ion-milled surfaces were compared. In this way, we were able to verify that the pores that we saw clearly once samples had been ion milled were already visible on mechanically polished surfaces. The GATAN 600 DuoMill™ did not produce significant changes of pore distribution or pore size at room temperature; it merely made the pores stand out more clearly.

To further verify the quality of our large diameter polishes, we used a GATAN Ilion™ edge mill to make polishes of a subset of 10 samples (duplicates from the set of 20 samples examined initially). The GATAN Ilion™ is a cross-beam ion mill that produces

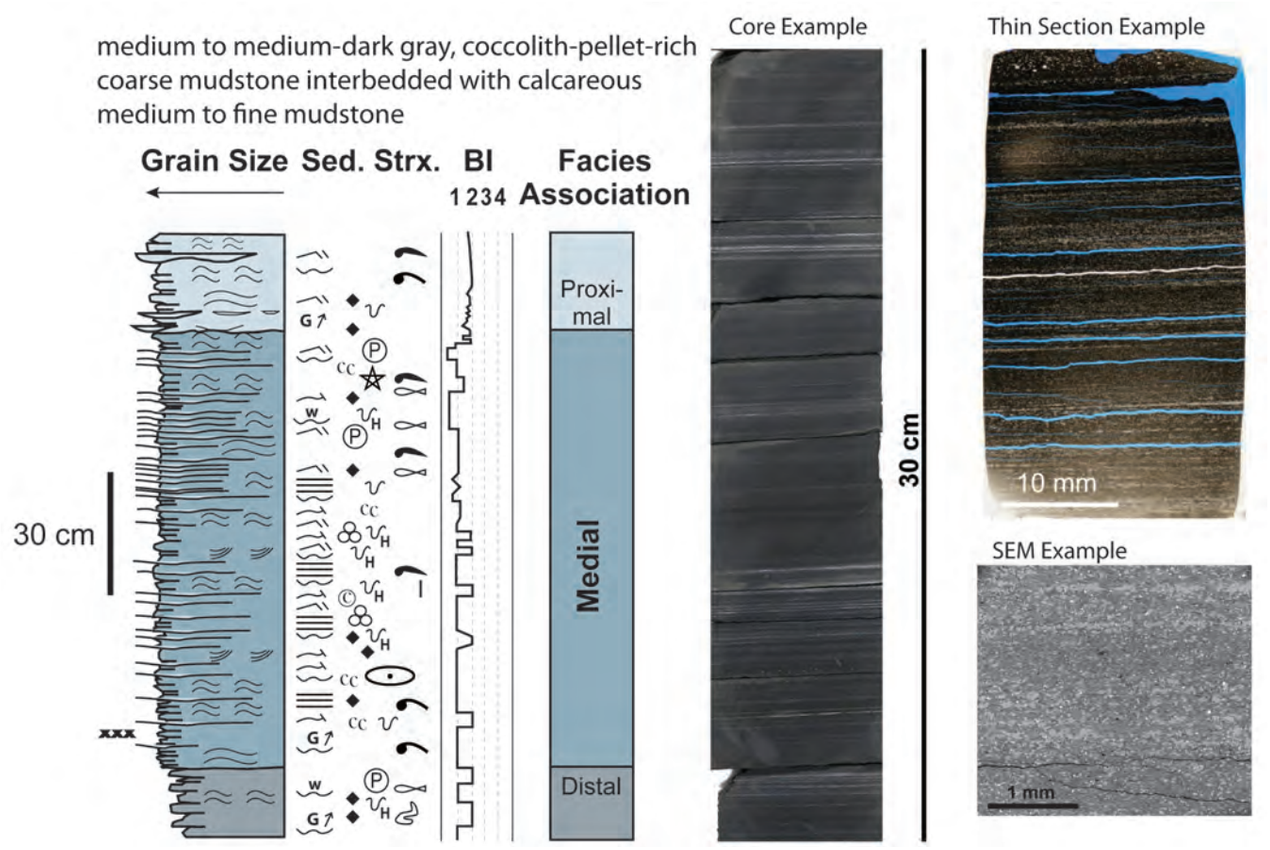

Figure 4. Overview of the medial facies association (FA-M). At left, a summary of sedimentary features observed in the FA-M (see Figure 2 for legend). In the middle, a typical example of FA-M in drill core. Note that in comparison to FA-D (Figure 7), original laminae are more common and better preserved. At right, photomicrographs of FA-M in a thin section (top) and an ion-milled sample (bottom). Grain types include fragments of *Pectinidae*, *Pteriidae*, and *Inoceramidae*; few disarticulated and scattered pieces of fish debris; coccolith-rich pellets and aggregates. Foraminifera and calcispheres are few to abundant in some beds and laminae. Foraminifera show various degrees of abrasion and their chambers are typically filled with calcite spar (~60–70%), organic material, authigenic clay minerals, and/or pyrite. The groundmass consists of compressed calcareous fecal pellets (~20–30% planktonic) that are mixed with clays, quartz silt, calcareous debris, volcanic ash components, and organic material. Submillimeter laminae (dominated by current-transported foraminifera tests) are clearly visible in the SEM image. Lamina disruptions may reflect shallow burrowing by tiny infauna (such as nematodes; Pike et al., 2001).

a high-quality polished area of about 0.3 to 2 mm^2, and the sample stage can be cooled with liquid nitrogen (LN2). In contrast to the Gatan 600 DuoMill™, the Gatan Illion™ has narrow and sharply focused argon ion beams and this makes its polishing action considerably more aggressive than that of the Gatan 600 DuoMill™. The milled area is substantially smaller than the area achieved with the Gatan 600 DuoMill™, but the generated surfaces are of excellent flatness.

The milled sample surfaces were examined without conductive coating with an *FEI* Quanta 400 FEG in low vacuum mode. We used non-coated samples because coating artifacts are in the same size range (nm to 10s of nm) as the pores that we were interested in observing. Operation in low vacuum mode does cause beam dissipation and loss of resolution, and we counteracted this effect by choosing close working distances and comparatively high beam voltages (typically 15 kV). The latter can potentially cause damage to organic material in the specimen, but was permissible because of the comparatively high maturity of the studied samples. Energy dispersive x-ray spectroscopy (EDS) was used to examine the composition of sedimentary particles.

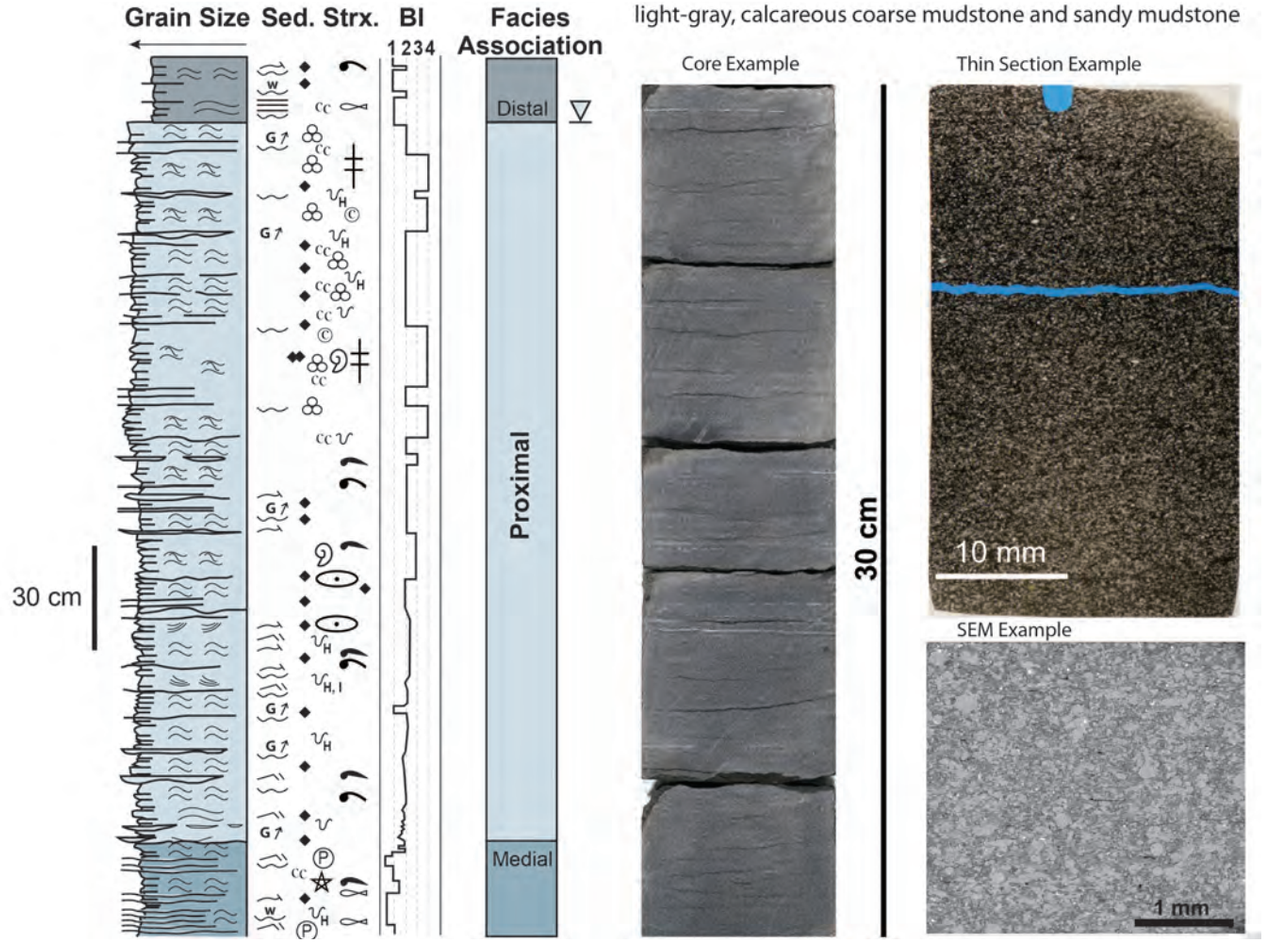

Figure 5. Overview of the proximal facies association (FA-P). At left, a summary of sedimentary features observed in the FA-P (see Figure 2 for legend). In the middle, a typical example of FA-P in drill core. At right, photomicrographs of FA-P in a thin section (top) and an ion-milled sample (bottom). Grain types include foraminifera, calcareous fecal pellets, and calcispheres, which are common to abundant (up to ~80%) in some beds, whereas radiolaria are sparse; foraminifera show various degrees of abrasion and their chambers are typically filled with diagenetic calcite (~50–100%), authigenic clay minerals, organic material, and/or pyrite. Larger grains are present in a groundmass of compressed planktonic fecal pellets that are mixed with clays, quartz silt, calcareous debris, volcanic ash components, and organic material. Early calcite cementation of this facies association is common. Original laminae may be visible, but considerable portions of the mudstone strata show disruption and homogenization by bioturbation. Hints of relict lamination are present in a mostly homogeneous-looking mudstone at thin section scale. The homogenization and mixing of components, likely due to bioturbation, is also observed in the SEM image.

EXPLORING ION MILLING ARTIFACTS

The GATAN Ilion™ has a liquid nitrogen (LN2) cooled sample holder, intended to help reduce thermal damage to the sample by the ion beam. From earlier tests with liquid nitrogen cooled samples under the ion beam we learned that cooling has distinct advantages for the ion milling of mudstones because it reduces or eliminates artifacts (illustrated in Figures 6–9) that can hamper accurate interpretation of porosity. For example, the well-known curtain effect that produces linear gashes in softer portions of ion-milled sections at room temperature can be greatly reduced or even eliminated with liquid nitrogen cooling (Figure 6). Thus, although cooling the sample is more labor intensive because of the need to periodically replenish the liquid nitrogen reservoir, it confers distinct benefits with regard to surface quality.

Table 1 Classification of Bioturbation (modified after Reineck, 1963; Potter et al., 1980; Droser and Bottjer, 1986), as used in Lazar et al. (2014). It should be noted that this scheme does not consider cryptobioturbation by meiofauna that obscures lamina boundaries and erases subtle sedimentary features (Schieber, 2003, 2014).

Bioturbation Index	Description
0	No burrows visible; primary sedimentary structures preserved
1	Beds continuous, but a few burrows; *weakly bioturbated*
2	Bed discontinuous, some burrows; *sparsely bioturbated*
3	Remnant bedding, burrows common, *mostly bioturbated*
4	Very little bed continuity, burrows abundant, *strongly bioturbated*
5	No remnant bedding, fully homogenized, *churned*

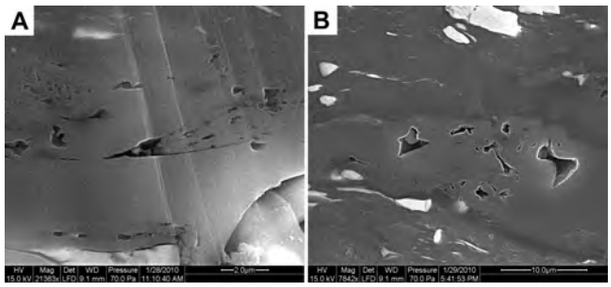

Figure 6. (A) Porous organic material milled at room temperature (5 kV beam voltage). (B) The same sample milled with liquid nitrogen cooled sample stage (5 kV beam voltage). Note absence of curtain effect and smooth surface in B.

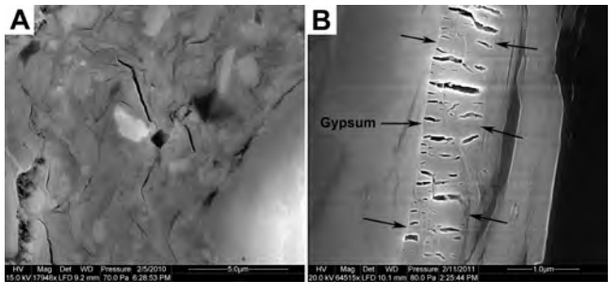

Figure 7. Dehydration shrinkage effects due to heating by milling beam. (A) Shrinkage crack development in smectite clays. Beam heating has removed water and caused shrinkage. (B) Gypsum-filled fracture (± vertical, arrows) with shrinkage cracks (± horizontal). Beam heating caused formation of calcium sulfate hemihydrate. The shrinkage occurs because gypsum has two water molecules per calcium sulfate molecule, whereas its hemihydrate has 0.5–0.8 water molecules per calcium sulfate molecule.

Figure 8. Heating-induced shrinkage of organic material (OM) in a pore space. Volume loss by driving out volatile components is interpreted to be caused by the heat from the milling beam, because the cracks were visible from the onset of SEM imaging. Heating by the SEM beam can also damage organic matter, but will be progressive as exposure to the SEM beam increases in duration. Typical results of this type of shrinkage are separation of the OM from OM-mineral interfaces (the two leftmost arrows) and at constrictions within OM areas (the two rightmost arrows).

Figure 9. A feature we call moat formation can be observed along the interfaces between organic material (OM) and pyrite (FeS_2). The OM near the interface is preferentially removed during milling, forming a "moat" (arrows). Our current explanation for this phenomenon is a chemical reaction between OM and sulfur ions produced during milling. Cooling the sample with liquid nitrogen suppresses this effect.

Other common heating-related artifacts include dehydration of hydrous minerals, such as smectites and gypsum (Figure 7), shrinkage of organic material (Figure 8), and moat formation around reactive constituents (Figure 9). All of these can be greatly reduced or eliminated through application of liquid nitrogen cooling.

To further test for artifacts, we also installed a liquid nitrogen cooled stage on one of our GATAN 600 DuoMill™ units. Cooling did not produce a noticeable improvement of the milled surface of the Eagle Ford samples, although we observed in other (non-Eagle Ford) samples that it significantly reduces shrinkage of hydrated clays (smectites) and other heat-sensitive minerals (Figure 7). We attribute this observation to the fact that our Eagle Ford samples range in maturity from about 1.2 to 1.5 % R_o, approximately reflecting burial temperatures between 120 and 180°C (e.g., Peters and Cassa, 1994). Temperature measurements with a non-contact infrared thermometer through the viewing port of the GATAN 600 DuoMill™ sample chamber suggest surface temperatures in the 120–140°C range for samples milled at 5 kV. We assume that because the examined samples had already experienced comparable heating during burial, ion milling is unlikely to add thermal damage to the sample surfaces. In immature to early mature samples, on the other hand, thermal damage should be expected and liquid nitrogen cooling of the sample is advisable to avoid artifacts. If our GATAN 600 DuoMill™ had inflicted thermal damage, that effect would have been readily apparent by comparing images of similar features. The maturity of the samples in addition to effective heat dissipation in the GATAN 600 DuoMill™ (sample rotates under beam) appears to have been sufficient to prevent heat-induced sample damage at room temperature milling in the case of Eagle Ford Shale samples. Thus, after extensive testing the conclusion is that we operated our equipment in a way that minimized/eliminated thermal damage to organic material in these samples and that the reported pores are largely true representations of pore spaces within these rocks.

Pore Types

For description of porosity we follow the approach outlined by Schieber (2010, 2013). We distinguished framework pores (pores defined by adjacent mineral grains), shelter pores, organic matter pores, and secondary dissolution pores. The term "framework pore" as used here is comparable to "matrix pore" as used by Rine et al. (2013) or to the term "interparticle pore" as originally defined by Choquette and Pray (1970) and more recently adopted for mudstones by Loucks et al. (2012). Shelter pores fall into the intraparticle pore category of Choquette and Pray (1970).

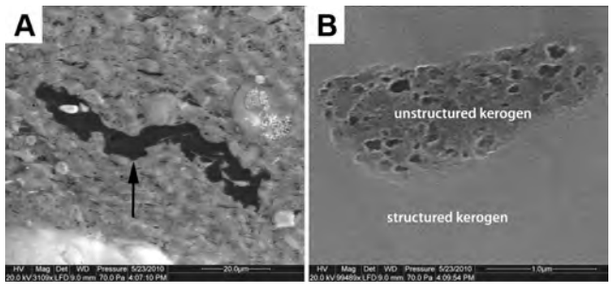

Figure 10. At left (A), a piece of marine plant matter (structured kerogen, black). In this particular example the plant matter has morphological pores (openings that existed when it grew), and these pores are now filled with amorphous kerogen. The image at right (B) shows the contrast in porosity between the structured plant matter organic material (OM) and the amorphous OM that occupied this open space later on. The latter is full of nm-scale pores, whereas the former is free of pores.

Pores in organic material (OM) are ubiquitous in all samples, but a distinction needs to be made between structured kerogen, unstructured (amorphous) kerogen, and migrated bitumen (e.g., Bohacs et al., 2013). Structured kerogen is OM that preserves morphologic features of the original phytoclast, such as algal cysts or spore casings. Unstructured or amorphous kerogen originates from bacterial reworking of lipid-rich algal debris (Peters and Moldowan, 1993). Bitumen is found both absorbed in kerogen and filling open spaces (inter- and intra-granular pores; e.g., foraminifer chambers and other fossil cavities). Structured kerogen is devoid of pores in the samples examined (Figure 10), whereas unstructured kerogen contains them abundantly (e.g., Schieber, 2010, 2013). Bitumen can host pores when it has been heated and transformed into pyrobitumen when these rocks reached the gas window (e.g., Bohacs et al., 2013).

Total Organic Carbon

Total organic carbon (TOC) content was measured after powdered whole samples were reacted with HCl and then combusted in a LECO elemental analyzer. Values of TOC concentrations are reported as weight percent (wt. %) of whole rock.

OBSERVATIONS

Facies Associations and Their Characteristics

Three facies associations—"distal," "medial," and "proximal"—have been recognized in the Eagle Ford mudstones examined in this study. The key attributes of these three facies associations are summarized next.

Distal facies association (FA-D)—argillaceous fine mudstone and calcareous fine to medium mudstone FA-D comprises very dark to dark gray, continuous, wavy-parallel to discontinuous, wavy-parallel-laminated, argillaceous fine mudstone to calcareous fine to medium mudstone (Figure 3). Few wave ripples and scours are present, whereas graded beds, potential wave-enhanced sediment-gravity-flow beds (Macquaker et al., 2010), current ripples, and planar beds are very sparse to sparse (Bohacs et al., 2011; Lazar et al., 2015). The bioturbation index (Table 1) is commonly 1 (to 2); trace fossils include *Planolites*, *Chondrites*, and mantle and swirl (sensu Lobza and Schieber, 1999). Additional components of this facies association include low to moderate faunal diversity with few fragments of *Inoceramidae*, scattered fish scales, and pyritized fish bones as well as scattered foraminifera, calcispheres, and sparse to common fecal pellets. Foraminifer tests constitute up to 50% of the framework grains in mudstones present in the intervals directly above flooding surfaces and commonly make 15–20% of the framework grains elsewhere. Foraminifer tests are mostly filled with calcite spar (~90%), authigenic clays, and organic material. Foraminifera are scattered through a groundmass that consists of compressed calcareous fecal pellets (~20–30% planktonic) and a mixture of clays, quartz silt, calcareous debris, volcanic ash components, and organic material. Common to abundant pyrite nodules and pyritized burrows also occur in some intervals. Total organic carbon content varies from 3 to 7 wt. %.

Medial facies association (FA-M)—interbedded coccolith pellet-rich coarse mudstone and calcareous medium to fine mudstone FA-M consists of medium to medium-dark gray, discontinuous, wavy-parallel to discontinuous, curved-non-parallel to discontinuous, wavy-non-parallel-laminated, coccolith pellet-rich coarse mudstone interbedded with calcareous medium to fine mudstone (Figure 4). Potential wave-enhanced sediment-gravity-flow beds and scours are few, whereas wave ripples, current ripples, and graded beds are sparse (Bohacs et al., 2011; Lazar et al., 2015). Bioturbation index typically varies between 1 and 2; trace fossils include *Planolites*, *Chondrites*, and *Helminthopsis*. Faunal diversity is moderate and includes fragments of *Pectinidae*, *Pteriidae*, and *Inoceramidae*. Few disarticulated and scattered fish debris, pyritized burrows, and phosphatic nodules are present in some intervals. Coccolith-rich pellets and aggregates, foraminifera, and calcispheres are few to abundant in some beds and laminae; foraminifera show various degrees of transport and reworking and their chambers are typically filled with calcite spar (~60–70%), OM, authigenic clay minerals, and/or pyrite (Figure 8). The groundmass consists of compressed calcareous fecal pellets (~20–30% planktonic) that are mixed with clays, quartz silt, calcareous debris, volcanic ash components, and OM. Total organic carbon content ranges from 2 to 6 wt. %.

Proximal facies association (FA-P)—calcareous coarse mudstone and sandy mudstone This FA is composed of light gray, discontinuous, wavy-non-parallel to discontinuous, curved-non-parallel-laminated, calcareous coarse mudstone to sandy mudstone with thick- and thin-wall bivalves, and horizontal to inclined burrows (Figure 5). Scours are common, wave ripples are few, and graded beds are sparse (Bohacs et al., 2011; Lazar et al., 2015). Bioturbation index typically varies between 2 and 4; trace fossils include *Planolites*, *Phycosiphon*, and *Teichichnus*. Foraminifera, calcareous fecal pellets, and calcispheres are common to abundant (up to ~80%) in some beds, whereas radiolaria are sparse; foraminifera show various degrees of transport and reworking and their chambers are typically filled with diagenetic calcite (~50–100%), authigenic clay minerals, OM, and/or pyrite. Framework grains are present in a groundmass of compressed planktonic fecal pellets that are mixed with clays, quartz silt, calcareous debris, volcanic ash components, and OM. Early calcite cementation of this facies association is common. Volcanic ash components are not as abundant as in FA-D and FA-M. Total organic carbon content ranges from 1 to 4 wt. %.

Pore Types

SEM examination of the 20 samples available for this study indicates the presence of pores associated with OM, pores defined by mineral frameworks (carbonate and clay), and pores developed in the infills of microfossil chambers. SEM examination also indicates that pore development is heterogeneous in the Eagle Ford Shale and depends on mudstone composition.

Pores associated with organic material (OM) We observed two types of pores associated with OM: (1) an abundance of smaller pores in the 10–50 nm range and (2) a superimposed small population of larger pores in the 100–1000 nm range (Figure 11). The pore structure of a sponge used for cleaning purposes makes for a good macroscopic analog, and the terms "foam" pores and "bubble" pores have previously

been suggested for the smaller pores and the larger pores, respectively (Schieber, 2010, 2013). Given that the nominal spatial resolution of our SEM is approximately 2 nm, observing the smallest OM pores poses a challenge. In our best images, however, we were able to resolve pores as small as 5 nm in size. Our images also captured what we interpret to represent pore throats between larger pores, which suggest that the pores are connected. As discussed later, we confirmed this interpretation by serial sectioning several samples with our GATAN Ilion ion mill.

Amorphous OM is pervasive throughout the rock matrix and occurs in interstitial spaces between carbonate and clay grains as well as in cavities provided by microfossils. The pore structure of this OM is the same, regardless of where it is found (Figure 12). When it occurs as infills of foraminifer chambers, the circular shape of the bubble pores is very suggestive of gas bubbles that originally formed in a liquid phase (Figure 13). As illustrated in Figure 13, the amount of bubble pores in the OM fill of a calcisphere is approximately 50%, and the amount of visible foam pores in the intervening organic matrix is approximately 20%, making for about 60% pore space in the organic infill of the calcisphere. This type of pores has been observed in all three facies associations, but is more commonly observed in the distal and medial facies associations.

Carbonate framework (CF) pores CF pores are defined by carbonate grains that form a supportive framework with triangular and polygonal interstitial pores between the grains. These grains are mostly microfossil and nannofossil debris that is scattered,

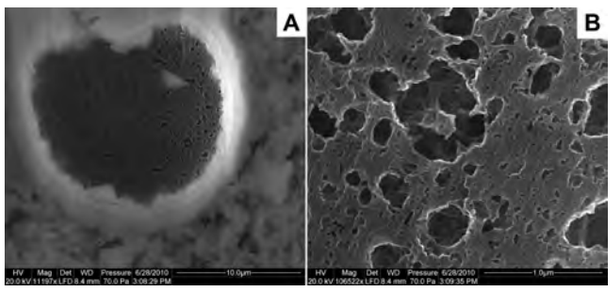

Figure 11. At left (A), a foraminifer chamber filled with organic material (OM) in the distal facies association. At right (B), SEM detail of the OM fill of this foraminifer chamber. The OM shows a foam-pore background in the 10–50 nm range and a second population of bubble pores in the 100–1000 nm range. Likely pore throats are visible at depth in several of the larger pores, an observation that indicates to us that the pores are most likely interconnected.

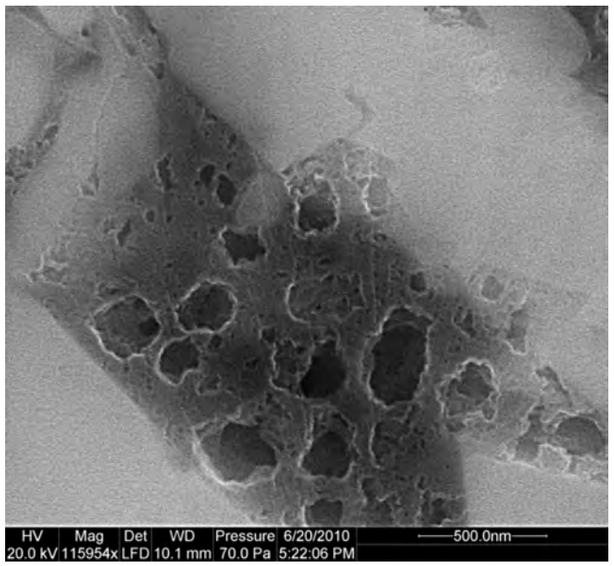

Figure 12. SEM detail illustrating foam and bubble pores in the organic material (OM) fill that occurs between calcareous fossil debris in the medial facies association. Foam pores are on the order of 10–50 nm in size, and the superimposed bubble pores are in the 100–500 nm size range. Close inspection of the SEM image suggests interconnectedness of the pores.

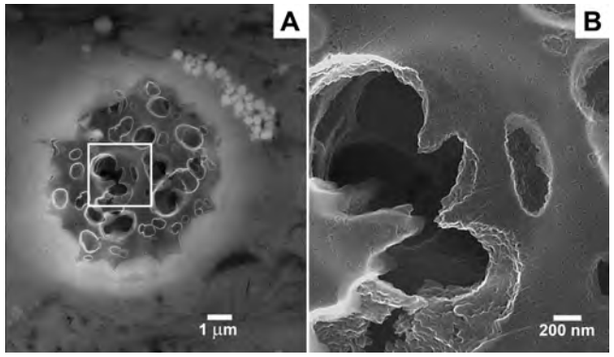

Figure 13. At left (A), organic material (OM) fill of a calcisphere from the medial facies association. At right (B), enlargement of the region outlined by the white square at left. Notice the presence of large bubble pores and "in-depth" connections between the large pores; notice also the presence of abundant smaller pores in the organic matrix.

aligned, or concentrated in fecal pellets. The most commonly observed CF pore type was in calcareous fecal pellets that consist of a support framework of carbonate fossil debris. CF pores also occur within the mudstone matrix wherever multiple carbonate grains

come into contact with each other. These framework pores are in many places filled or partially filled with OM that in itself is porous (OM pores). The OM fill of the associated CF can be as porous (Figure 12) as that inside foraminifer chambers (Figure 11). Where hydrocarbon migration/expulsion occurred, CF pores may have been entirely cleared of their OM fill, or they may only show a thin OM lining along the pore margins. CF pores are very abundant in calcareous fecal pellets, which, in turn, typically range in abundance from sparse in the FA-P to common in the FA-M. Examples of CF pores are shown in Figures 14–16.

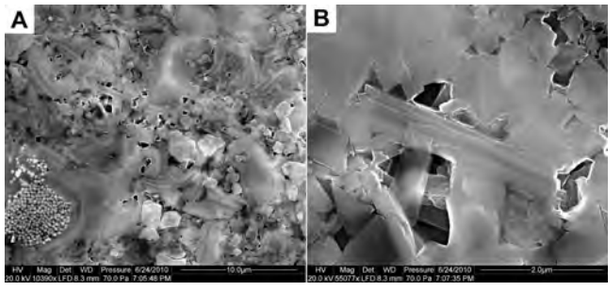

Figure 14. At left (A), abundant large pores in the 500–1000 nm size range in a groundmass rich in calcareous debris from the medial facies association. The organic material (OM)-fills of carbonate framework (CF) pores have developed porosity and in places the OM has been entirely removed. At right (B), close-up of CF pores from prior image. The pores show in-depth connections, which suggest pore interconnectedness.

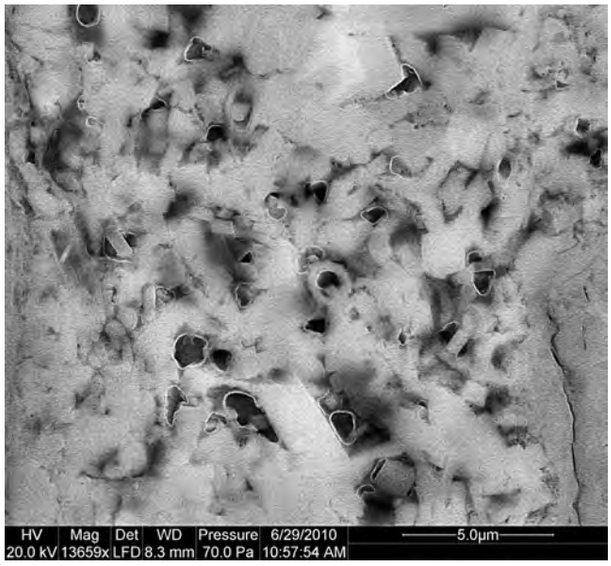

Figure 15. Abundant large carbonate framework (CF) pores in the 500–1000 nm size range in a groundmass rich in calcareous debris, observed in a sample from the distal facies association.

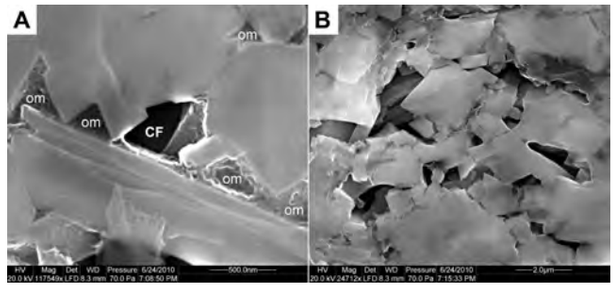

Figure 16. At left (A), SEM close-up of pores in the organic material (OM) fill of carbonate framework (CF) pores from the medial facies association. Smaller CF pores tend to be filled with OM and have abundant foam pores (10–50 nm). Larger CF pores tend to be almost free of OM fill. We interpret this to indicate that viscous hydrocarbons generated during maturation were able to migrate out of the larger pores, but were not able to overcome the friction within smaller pores. At right (B), another SEM view (same sample) of well-developed CF pores with in-depth connectivity between pores.

Phyllosilicate framework (PF) pores PF pores are very common in the diagenetic clay infills of foraminifer chambers and are a common element in the silicate-rich groundmass especially of the distal (FA-D) and medial (FA-M) facies associations. Their overall abundance appears to be lower in the proximal (FA-P) facies association although some rather large PF pores have been observed in this facies association. PF pores are ubiquitous in the mudstone groundmass and consist of triangular openings (Figure 17) that are defined by a lattice work of randomly oriented clay mineral platelets (Schieber, 2010). These triangular pores range in size from a few nanometers to more than a micron. They are best developed in pressure shadows adjacent to larger compaction-resistant grains (e.g., silt, sand, fossil debris) and in spaces between such grains. The defining clay-mineral platelets, typically a few microns in size, appear to have multiple origins. In places they can show textures suggestive of detrital origin, such as bending and splintering due to compaction, as well as piercing and differential compaction when oriented near-vertical (e.g., Schieber, 2010, 2013), but the infills of foraminifer chambers also point to a common diagenetic clay component.

In the examined samples, PF pores are typically filled with OM, similar to what is seen in the case of CF pores. The OM fill shows exactly the same kind of pore structure as observed in the OM that fills the CF pores (Figures 18, 19). PF pores like those illustrated in Figure 17 may constitute the bulk of available porosity in mudstone beds that received a strong volcanic ash contribution and where clays are abundant (Figures 20, 21).

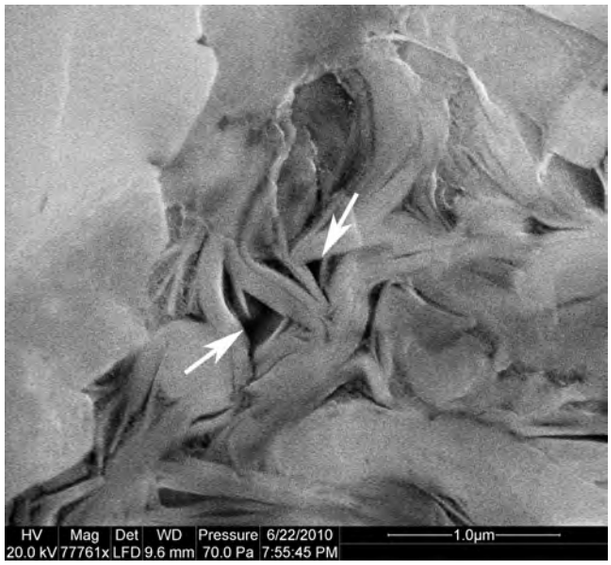

Figure 17. Triangular phyllosilicate framework (PF) pores (arrows) observed in the pressure shadows of silt-sized grains present in the medial facies association. In this particular image they are simply empty pores, but in many instances this pore type is filled with organic material that has the pore structure (foam and bubble) illustrated in Figure 11.

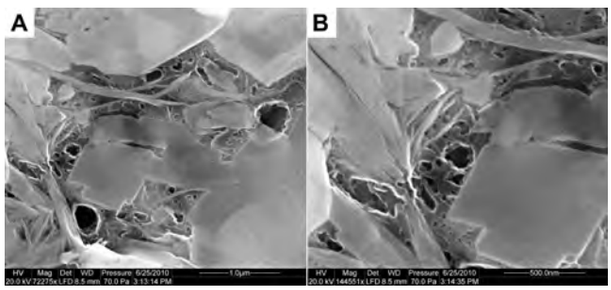

Figure 18. Organic material (OM) fill with OM pores in phyllosilicate framework (PF) pores from the distal facies association. At left (A), OM mingled with clays fills interstitial spaces between larger grains. OM shows abundant small foam pores (10–50 nm) and a small number of possibly interconnected large bubble pores (100–500 nm). At right (B), a close-up from the left SEM image. Notice that interstitial spaces in PF pores are filled with OM that itself is porous.

Shelter porosity and diagenetic clay Shelter pores are commonly observed in tests of foraminifera (Figures 20, 21). These tests are commonly multichambered and range in size from tens to hundreds of microns. The amount of foraminifer tests in a given sample varies and ranges from 10 to 80% in the examined mudstones, commonly increasing in abundance from the distal to the proximal facies association (see earlier detailed FA characterization). Chambers of foraminifera can be filled with diagenetic calcite, diagenetic

Figure 19. Example of phyllosilicate framework (PF) pores in the proximal facies association (SEM image). PF pores can be filled to various degrees with porous organic material (OM).

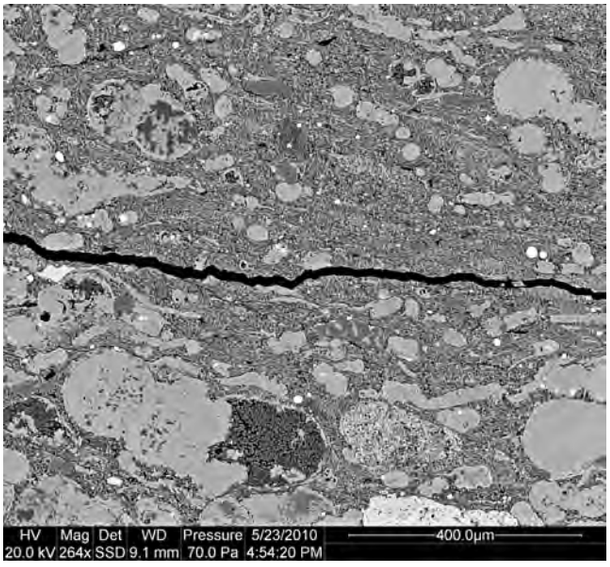

Figure 20. Backscatter SEM image of a mudstone fabric homogenized by bioturbation from the medial facies association. Note the presence of both calcite-filled (light gray) and clay-filled (dark gray) tests of foraminifera.

clays (kaolinite and/or Mg-chlorite; Figure 21), pyrite framboids, and OM. These infills can occur together, or may be the sole fill of a given chamber. Most commonly, chambers are entirely filled with calcite. An increased amount of diagenetic clay filling the chambers has been observed in mudstones rich in volcanic ash. SEM-based EDS analysis as well as

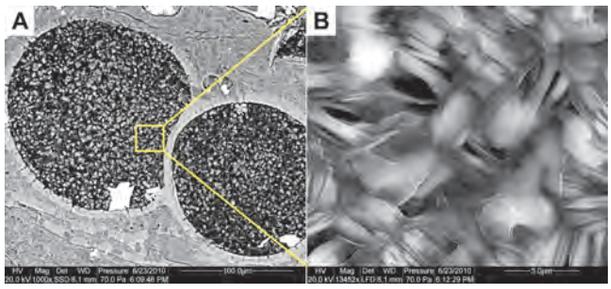

Figure 21. At left (A), an SEM image of chambers of foraminifera filled with diagenetic kaolinite from the medial facies association. At right (B), a close-up of this clay fill (yellow rectangle in A) that shows phyllosilicate framework pores between stacks of kaolinite platelets.

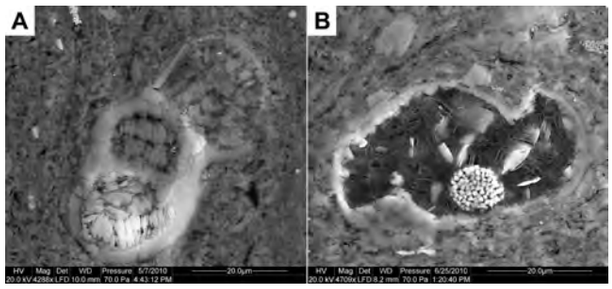

Figure 22. At left (A), a secondary electron SEM image of a clay-filled foraminifer from the medial facies association. Notice that diagenetic clays dominate the chamber space and that interstitial porosity is minor. Pores are either of the phyllosilicate framework (PF) type or the organic material (OM) type, with OM trapped in interstitial areas. At right (B), a secondary electron SEM image of a clay-OM filled, partially collapsed foraminifer test; the clay to OM ratio is about 1 or less and large pores are visible in the OM.

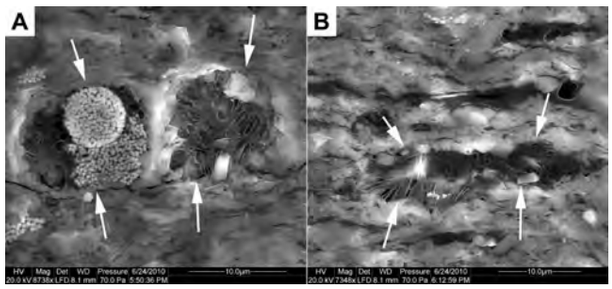

Figure 23. At left (A), an SEM image of a two-chambered foraminifer in the proximal facies association. Notice that the right chamber is filled with clay/organic material (OM) and that large OM pores are present within the phyllosilicate framework (PF) framework. The left chamber is filled with pyrite and clay-free OM with large pores. The foraminifer walls are partially dissolved (white arrows). At right (B), an SEM image of a deformed clay/OM lump (white arrows) with large OM pores within the PF. The texture is identical to that seen in the foraminifer fill at left. This suggests that the clay/OM lump started out as a filled foraminifer and that later on the foraminifer walls were dissolved.

textural features suggest that these clays are largely kaolinite and Mg-chlorite. The clays form a random framework of clay-mineral stacks (Figure 21), and pore spaces are preserved within this framework (Figure 22). Porous OM typically fills in between diagenetic clays and may also be a sole fill material. There is also evidence of wall dissolution, which is associated with collapse/compaction of the foraminifer structure and its interior fill. Tubular coccolith structures also provide shelter porosity. These pores can be open, but typically are filled with porous OM. As illustrated earlier, the best and largest pore development is found in the infills of microfossil chambers (Figures 11, 13) where porosities in excess of 50% can occur (Figure 13).

Carbonate dissolution Carbonate dissolution is widespread in the Eagle Ford Shale samples studied here; however, this process did not produce noticeable secondary porosity (Schieber, 2010, 2013). The clearest evidence for carbonate dissolution during burial diagenesis in these mudstones is provided by the partial or complete dissolution of walls of foraminifer chambers leaving behind deformed clay/OM lumps (Figures 22, 23).

Deformed clay/OM lumps with large OM pores are a common feature in most samples (Figure 23). There is a complete spectrum from examples of well-preserved foraminifer chambers filled with clay and OM (Figure 21), to examples of partial dissolution of chamber walls (Figure 23A), to deformed clay/OM lumps (Figure 23B). The latter are therefore interpreted as remains of dissolved foraminifera and attest to dissolution of carbonate at some time during burial. The composition of these dissolution residuals indicates that the amorphous kerogen (bitumen) fills were emplaced prior to dissolution of the foraminifera chamber walls. Thus, dissolution may have approximately coincided or overlapped with hydrocarbon formation and may represent pH lowering as organic acids were generated during burial diagenesis of organic matter. Research on oil field brines and pore water evolution during burial suggests that the initial stages of smectite transformation are followed by (and overlap with) decarboxylation of kerogen and a buildup of carboxylic and phenolic acids in

the temperature range from 80 to 120°C (MacGowan and Surdam, 1990; Hayes, 1991; Surdam et al., 1991). In sandstones this stage is associated with formation of secondary porosity and destruction of carbonates (Hayes, 1991). It seems therefore a reasonable conjecture that the carbonate dissolution observed in Figure 23 is likewise linked to organic acid formation. Because the initial amount of organic matter in a shale will place limits on the amount of organic acids that can be generated in this way, it seems likely that in organic-rich shales this can lead to considerable amounts of secondary porosity. How important dissolution was in the Eagle Ford Shale for generation of porosity is uncertain. The bulk of the CF pores observed did not show signs of significant dissolution. This could reflect the fact that this carbonate-rich sediment had a high capacity to buffer acidity without the effect becoming very prominent.

DISCUSSION

Facies Associations and Porosity

Porosity in the examined Eagle Ford Shale samples is a function of the framework-grain and groundmass types and distributions, which, in turn, vary among facies associations. It is then reasonable to investigate the link between facies associations and porosity types and distribution.

The three facies associations, "distal" (FA-D), "medial" (FA-M), and "proximal" (FA-P), recognized within the Eagle Ford Shale form successions that have a characteristic stacking pattern (Figure 24), which we interpret to represent distinct parasequences (e.g., Bohacs, 1998; Bohacs et al., 2014; Lazar et al., 2015). All attributes within a facies association succession record an upward increase in sediment grain size and reworking, sedimentation rates, and oxygenation level (Figure 24). We interpret the three facies associations as a result of mud accumulation under variable depositional conditions on the distal, medial, and proximal portions of a storm-wave-dominated shelf, respectively (Figure 24). These sub-environments experienced significant variations in primary biogenic production, bottom-energy and oxygen levels, as well as sediment accumulation modes and rates (Figure 24), which result in significant variations in the type and distribution of framework grains.

The different pore categories observed in the Eagle Ford Shale samples examined in this study under SEM include intergranular pores defined by clay flakes and carbonate particles, intra-granular pores associated with foraminifer chambers, and pores within OM. As illustrated in Figures 11–23, these pores are not uniformly distributed. In many instances, framework and shelter pores are filled with OM that has developed pores due to maturation (Figures 16, 18, 19). The large bubble pores present in OM suggest that hydrocarbon liquids were left behind in or migrated into these rocks following petroleum generation and that the bubbles developed as these mudstones experienced additional thermal stress. These larger OM pores show indications of deeper seated interconnection on ion-milled surfaces (e.g., Figures 11, 13) and in 3-D image stacks. Because the OM postdates the framework and shelter pores, we actually have a pore-in-pore situation where we can get a mental image of porosity before the onset of hydrocarbon generation, as well as examine porosity in its present state.

Porosity developed in all three facies associations. For example, the largest pores and highest porosity occur in shelter pores, such as foraminifer tests (e.g., FA-M and FA-P; Figures 22, 23). The framework of crushed carbonate debris in planktonic fecal pellets shows intermediate levels of porosity (e.g., FA-M, Figure 16), and the silicate-rich matrix (or groundmass) that encloses these other components has the smallest pores (e.g., FA-M and FA-D; Figures 17, 18). Matrix porosity is strongly dominated by the pores in OM (e.g., FA-M; Figure 22), whereas fecal pellets also show abundant open framework pores (e.g., FA-M; Figure 16). It is our current assumption that as the proportion of calcareous fecal pellets increases, so should the overall porosity of a given sample.

Our pore observations are made on ion-milled surfaces from only 20 samples. With this caveat in mind, we propose here that within a facies association succession (i.e., parasequence), organic-hosted pores are more abundant in the distal facies association (when developed at higher thermal maturities) whereas inter- and intra-granular pores are likely most common in the proximal facies association. We further hypothesize that porosity develops best in medial portions of parasequences when all three porosity types are present (Figure 24). Cementation and pore occlusion by calcite has commonly been observed in the proximal facies association. This lower-porosity situation likely reflects the fact that the proximal facies association intervals are bounded above by flooding surfaces, commonly resulting in preferential cementation of their upper portions by microbial activity during periods of low sediment accumulation following flooding (e.g., Berner, 1980; Taylor and Macquaker, 2000; Lazar et al., 2015).

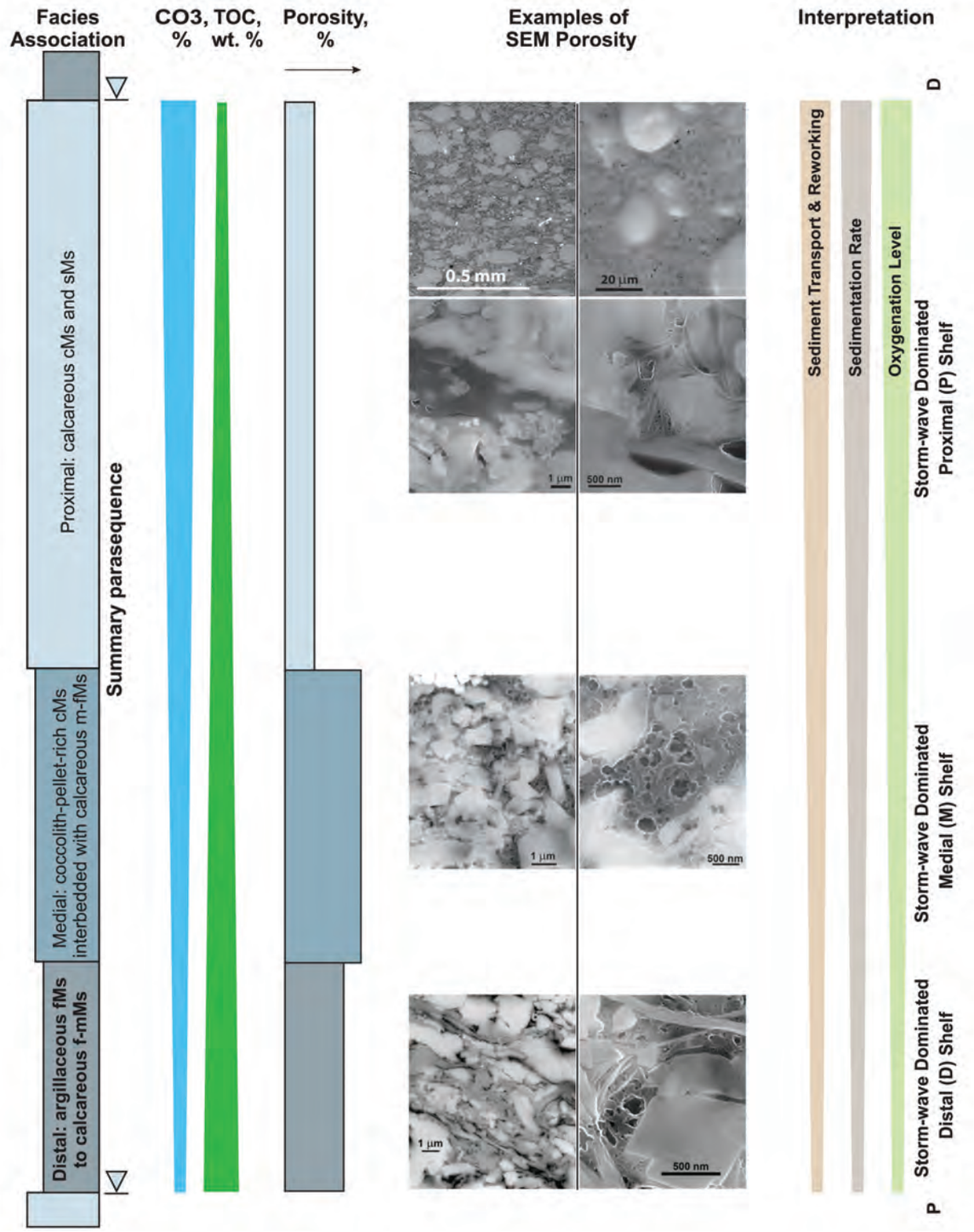

Figure 24. Summary of mudstone fabric and pore types in the context of parasequence development. It is our conjecture that in the distal facies association (FA), the higher abundance of clays leads to a fabric with a more planar character and that most of the porosity is confined to organic material (OM) and small framework pores. In contrast, in the medial facies, an abundance of calcareous fecal pellets (carbonate framework pores) and shelter porosity in foraminifer tests presumably leads, in combination with an abundance of OM pores, to a porosity optimum. In the proximal facies, even though carbonate framework pores are well developed, available porosity is interpreted to be lower because of the lower amount of OM and because of occlusion of pore space by carbonate cement.

Depositional Processes and Reservoir Quality

Given the observed heterogeneity of porosity, we hypothesize that processes that reorganize the various mudstone fabric components (Figure 25) are likely to have an impact on the overall porosity as well as the bulk permeability of a given mudstone. Given the size and geometrical arrangement of fabric components (Figure 25), this impact is not easily quantified with any precision, and for the time being we can only make suggestions based on our petrographic and sedimentologic observations. For example, rock components may be randomly arranged and mixed as they would be under the influence of strong bioturbation (Figure 26A). One could argue that when components of higher porosity (foraminifer chambers and fecal pellets) are enclosed in a matrix with smaller pores and less overall porosity, the matrix likely controls the overall permeability of the mudstone reservoir.

The interstitial nature of much of the OM observed here suggests that OM is a residual of an original fluid phase and as such most likely forms an intermeshed fabric of touching OM strands and lumps. Within this filigrane network, the interconnected small foam pores (10–50 nm) are most likely the locus of gas storage. If the large bubble pores (100–1000 nm) are connected in 3-D, then together with open framework pores they facilitate hydrocarbon migration within the rock volume. We argue that the spatial juxtaposition of bubble pores and foam pores makes for efficient transfer of hydrocarbon from storage (foam pores) to migration pathways (bubble pores and framework pores).

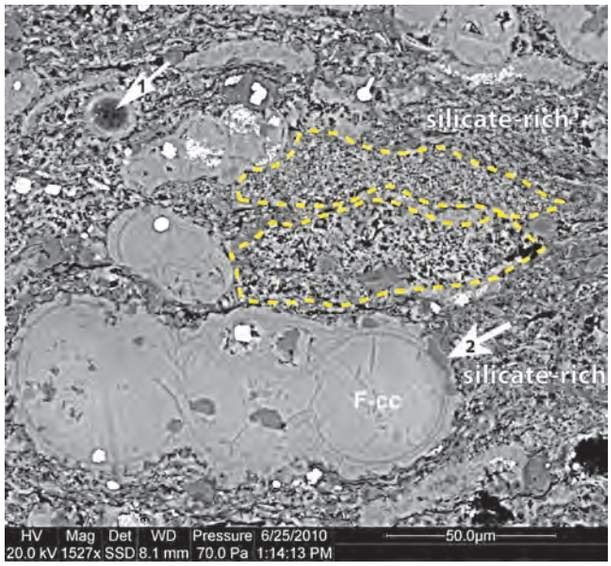

Figure 25. Backscatter SEM image of typical components of the rock fabric in the Eagle Ford Shale, as seen in the medial facies association: multi-chambered foraminifera filled with calcite (F-cc) or organic material (OM) (arrow 1) and deformed calcareous fecal pellets (planktonic; examples outlined by dashed yellow line) in a more silicate-rich matrix. Arrow 2 points to silica replacement of the wall of a foraminifera test.

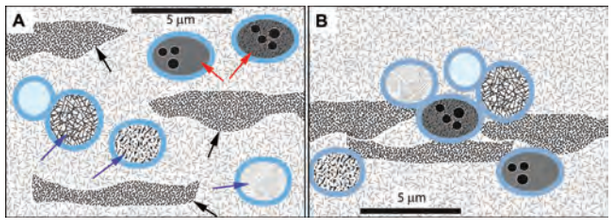

Figure 26. Cartoons illustrating the potential impact of current- or wave-induced particle sorting on reservoir performance. In (A), larger particles are surrounded by a low permeability matrix of clays, calcareous fossil debris, and organic material (OM). Red arrows point to OM-filled foraminifer tests (OM pores), blue arrows point to clay and OM-filled foraminifer tests (phyllosilicate framework [PF] and OM pores), and black arrows point to calcareous fecal pellets (CF and OM pores). In (B), these more porous components have been concentrated into thin lags and form continuous laminae.

Mud can be emplaced by currents in bedload (e.g., Schieber et al., 2007; Schieber and Southard, 2009; Schieber and Yawar, 2009; Plint et al., 2012), as well as in the presence of wave action (e.g., Chang and Flemming, 2013). Both processes invariably lead to sorting of grains into discrete laminae that reflect current strength as well as density differences of grains. The foraminifera-enriched laminae more commonly present in FA-M are likely of that origin (Figure 4). Laminae that show enrichment in calcareous fecal pellets are also present but less conspicuous. We speculate that abundant current- or wave-generated laminae of more porous particles (Figure 26B) may translate into higher permeability parallel to bedding, and when paired with fractures perpendicular to bedding could lead to enhanced reservoir performance.

CONCLUDING REMARKS

Multiple pore types occur in the Eagle Ford Shale in the gas maturity window. These include pores defined by mineral frameworks (clay and calcite), shelter pores in microfossil debris, and pores in OM. Commonly, framework and shelter pores are filled with OM that has developed both larger and smaller pores due to maturation. The development of these pores depends on mudstone composition.

The distribution of pore types is not uniform. Facies association is an important factor that influences bulk porosity. The observed variability in the attributes of the distal, medial, and proximal facies associations described here translates into significant variability of rock properties such as TOC and, based on our data, porosity. In turn, this variability likely controls the quality and distribution of mudstone intervals that are optimum sources and reservoirs of hydrocarbons in the Eagle Ford Shale. Our working hypothesis is that the medial facies association should have the best porosity development through a favorable combination of more abundant calcareous fecal pellets and OM versus clay content. The systematic arrangement of facies associations into parasequences provides the genetic framework for testing and predicting the best development of optimal reservoir facies in mudstone successions.

Depositional processes have a bearing on rock fabric and by extension on mudstone porosity as well as permeability. We hypothesize that rock fabric affects the permeability of rocks of otherwise equal composition. From that vantage point, randomizing higher porosity components in a lower porosity matrix should lead to lower permeability, whereas concentration of higher porosity components into laminae by current or wave action should enhance permeability parallel to bedding. In a silicate-rich matrix, framework elements like carbonate grains are less abundant, and the PF frameworks have a tendency to get flattened due to compaction. Consequently, the resulting mudstone should show reduced matrix porosity.

Capturing rock heterogeneity within shales is facilitated by the recognition and detailed description of key mudstone attributes, including texture, bedding, and composition, as well as of additional attributes such as physical sedimentary structures, degree of bioturbation, fossils, diagenetic components, grain origin, and color (e.g., Schieber, 1985, 1998, 1999; Bohacs, 1990, 1998; Lazar et al., 2015). In the case of the Eagle Ford Shale, identification and capture of mudstone heterogeneity enabled us to decipher past depositional conditions and environments. Within the stratigraphic context throughout a depositional basin, understanding of spatial heterogeneity in mudstone successions facilitates predictions of the quality and distribution of source, reservoir, and seal intervals.

ACKNOWLEDGMENTS

We would like to thank John Breyer for guiding this manuscript through the review process at AAPG, Wayne Camp and anonymous reviewers for constructive criticism in the AAPG review process, as well as Lee Esch, Joe Macquaker, and Rene Jonk for their insightful internal reviews at ExxonMobil. We would also like to thank ExxonMobil management for support and permission to release this information. Moreover, we would like to thank Corelab for permission to release information.

REFERENCES CITED

Adams, R. L., and J. P. Carr, 2010, Regional depositional systems of the Woodbine, Eagle Ford, and Tuscaloosa of the U.S. Gulf Coast: Gulf Coast Association of Geological Societies Transactions, v. 60, p. 3–27.

Berner, R. A., 1980, Early diagenesis: A theoretical approach: Princeton, New Jersey, Princeton University Press, 241 p.

Bohacs, K. M., 1990, Sequence stratigraphy of the Monterey Formation, Santa Barbara County: Integration of physical, chemical, and biofacies data from outcrop and subsurface: SEPM Core Workshop, v. 14, p. 139–200.

Bohacs, K. M., 1998, Contrasting expressions of depositional sequences in mudrocks from marine to non marine environs, *in* J. Schieber, W. Zimmerle, and P. Sethi, eds., Shales and mudstones: v. I, E. Schweizerbart'sche Verlagsbuchhandlung (Nagele u. Obermiller), p. 33–78.

Bohacs, K. M., O. R. Lazar, and T. M. Demko, 2014, Parasequence types in shelfal mudstone strata—Quantitative observations, lithofacies stacking patterns, and a conceptual link to modern depositional regimes: Geology, v. 42, p. 131–134.

Bohacs, K. M., J. D. Ottmann, O. R. Lazar, M. Dumitrescu, R. Klimentidis, J. Schieber, R. Montelli, C. Liu, and J. Shamrock, 2011, Genetic controls on the occurrence, distribution, and character of reservoir-prone strata of the Eagle Ford Group and related rock: HGS Annual Meeting.

Bohacs, K. M., I. O. Norton, D. Gilbert, J. E. Neal, M. Kennedy, W. Borkowski, M. Rottman, and T. Burke, 2012, The accumulation of organic-matter-rich rocks within an earth systems framework: The integrated roles of plate tectonics, atmosphere, ocean, and biota through the Phanerozoic, *in* D. Roberts and A. W. Bally, eds., Principles of geological analysis: Elsevier, p. 647–678, doi:10.1016/B978-0-444-53042--4.00023-6, #2532.

Bohacs, K. M., Q. R. Passey, M. Rudnicki, W. L. Esch, and O. R. Lazar, 2013, The spectrum of fine-grained reservoirs from "shale gas" to "shale oil"/ tight liquids: Essential attributes, key controls, practical characterization: IPTC 16676, p. 1–16.

Bostik, W. C., 1960, Micropaleontology of the upper Eagle Ford and lower Austin groups, Big Bend National Park, Texas: M.S. Thesis, Texas Technological College, 145 p.

Brett, C. E., and P. A. Allison, 1998, Paleontological approaches to the environmental interpretation of mudrocks, *in* J. Schieber, W. Zimmerle, and P. Sethi, eds., Mudstones and shales 1: Basin studies, sedimentology, and paleontology: Stuttgart, Schweizerbartsche Verlagbuchhandlung, p. 301–349.

Bryer, J. A., R. Denne, J. Funk, T. Kosanke, and J. Spaw, 2013, Stratigraphy and sedimentary facies of the Eagle Ford Shale (Cretaceous) between the Maverick Basin and the San Marcos arch, Texas, USA: AAPG Search and Discovery Article #50899.

Chang, T. S., and B. W. Flemming, 2013, Ripples in intertidal mud—A conceptual explanation: Geo-Marine Letters, v. 33, p. 449–461.

Choquette, P. W., and L. C. Pray, 1970, Geologic nomenclature and classification of porosity in sedimentary carbonates: AAPG Bulletin, v. 54, p. 207–250.

Dawson, W. C., and W. R. Almon, 2010, Eagle Ford Shale variability: Sedimentologic influences on source and reservoir character in an unconventional resource unit: Gulf Coast Association of Geological Societies Transactions, v. 60, p. 181–190.

Donovan, A. D., and T. S. Staerker, 2010, Sequence stratigraphy of the Eagle Ford (Boquillas) Formation in the subsurface of South Texas and outcrops of West Texas: Gulf Coast Association of Geological Societies Transactions, v. 60, p. 861–899.

Driskill, B., J. Walls, J. DeVito, and S. W. Sinclair, 2013, Applications of SEM imaging to reservoir characterization in the Eagle Ford Shale, south Teas, U.S.A., *in* W. Camp, E. Diaz, and B. Wawak, eds., Electron microscopy of shale hydrocarbon reservoirs: AAPG Memoir 102, p. 115–136.

Droser, M. L., and D. J. Bottjer, 1986, A semiquantitative field classification of ichnofabric: Journal of Sedimentary Research, v. 56, p. 558–559.

Goldhammer, R. K., and C. A. Johnson, 2001, Middle Jurassic-Upper Cretaceous paleogeographic evolution and sequence-stratigraphic framework of the northwest Gulf of Mexico rim, *in* C. Bartolini, R. Buffler, and A. Cantu-Chapa, The Western Gulf of Mexico Basin: Tectonics, sedimentary basins, and petroleum systems, AAPG Memoir 75, p. 45–81.

Halbouty, M. T., A. A. Meyerhoff, R. E. King, R. H. Dott, D. Klemme, and T. Shabad, 1970, World's giant oil and gas fields, geologic factors affecting their formation, and basin classification [Part 1], *in* M. Halbouty, ed., Geology of giant petroleum fields: AAPG Memoir 14, p. 502-528.

Hayes, J. B., 1991, Porosity evolution of sandstones related to vitrinite reflectance: Organic Geochemistry, v. 17, p. 117–129.

Hentz, T. F., and S. C. Ruppel, 2011, Regional stratigraphic and rock characteristics of Eagle Ford Shale in its play area: Maverick Basin to East Texas Basin: AAPG Search and Discovery Article #10325.

Jennings, D. S., and J. Antia, 2013, Petrographic characterization of the Eagle Ford Shale, south Texas: Mineralogy, common constituents, and distribution of nanometer-scale pore types, *in* W. Camp, E. Diaz, and B. Wawak, eds., Electron microscopy of shale hydrocarbon reservoirs: AAPG Memoir 102, p. 101–113.

Lazar, O. R., K. M. Bohacs, J. H. S. Macquaker, J. Schieber, and T. Demko, 2014, Capturing key attributes of fine-grained sedimentary rocks in outcrops, cores, and thin sections: Nomenclature and description guidelines: Journal of Sedimentary Research, v. 85, p. 230–246.

Lazar, R. O., K. Bohacs, J. Macquaker, J. Schieber, and T. Demko, 2013, Classification and description guidelines for the spectrum of fine-grained sedimentary rocks: Simplicity and order out of chaos: AAPG Search and Discovery Article #90142, AAPG Annual Convention and Exhibition, Pittsburgh, Pennsylvania.

Lobza, V., and J. Schieber, 1999, Biogenic sedimentary structures produced by worms in soupy, soft muds: Observations from the Chattanooga Shale (Upper Devonian) and experiments: Journal of Sedimentary Research, v. 69, p. 1041–1049.

Loucks, R. G., R. M. Reed, S. C. Ruppel, and U. Hammes, 2012, Spectrum of pore types and networks in mudrocks and a descriptive classification for matrix-related mudrock pores: AAPG Bulletin, v. 96, p. 1071–1098.

Lundquist, J. J., 2000, Foraminiferal biostratigraphic and paleoceanographic analysis of the Eagle Ford, Austin, and lower Taylor groups (middle Cenomanian through lower Campanian) of central Texas: Ph.D. Dissertation, University of Texas, 545 p.

Macquaker, J. H. S., S. J. Bentley, and K. M. Bohacs, 2010, Wave-enhanced sediment-gravity flows and mud dispersal across continental shelves: Reappraising sediment transport processes operating in ancient mudstone successions: Geology, v. 38, p. 947–950.

MacGowan, D. B., and R. C. Surdam, 1990, Carboxylic acid anions in formation waters, San Joaquin Basin and Louisiana Gulf Coast, USA—Implications for clastic diagenesis: Applied Geochemistry, v. 5, p. 687–701.

Miller, R. W., 1990, The stratigraphy and depositional environment of the Boquillas Formation of southwest Texas: M.S. Thesis, University of Texas, Arlington, 156 p.

Peters, K. E., and J. M. Moldowan, 1993, The biomarker guide: Interpreting molecular fossils in petroleum and ancient sediments. Englewood Cliffs, New Jersey, Prentice-Hall, 363 p.

Peters, K. E., and M. R. Cassa, 1994, Applied source rock geochemistry, *in* L. B. Magoon and W. G. Dow, eds., The petroleum system—From source to trap: AAPG Memoir 60, p. 93–120.

Pike, J., J. M. Bernhard, S. G. Moreton, and I. B. Butler, 2001, Microbioirrigation of marine sediments in dysoxic environments: Implications for early sediment fabric formation and diagenetic processes: Geology, v. 29, p. 923–926.

Plint, A. G., J. H. S. Macquaker, and B. L. Varban, 2012, Bedload transport of mud across a wide, storm-influenced ramp: Cenomanian–Turonian Kaskapau Formation, Western Canada Foreland Basin: Journal of Sedimentary Research, v. 82, p. 801–822.

Potter, P. E., J. B. Maynard, and W. A. Pryor, 1980, Sedimentology of shale: Study guide and reference source: New York, Springer-Verlag, 303 p.

Powell, J. D., 1965, Late Cretaceous platform-basin facies, northern Mexico and adjacent Texas: AAPG Bulletin, v. 49, no. 5, p. 511–525.

Reineck, H. E., 1963, Sedimentgefüge im Bereich der südlichen Nordsee: Abhandlungen der Senckenbergischen Naturforschenden Gesellschaft 505, p. 1–138.

Rine, J. M., E. Smart, W. Dorsey, K. Hoogan, M. Dixon, and J. Schieber, 2013, Comparison of porosity distribution within selected North American shale units by SEM examination of argon-ion-milled samples, *in* W. Camp, E. Diaz, and B. Wawak, eds., Electron microscopy of shale hydrocarbon reservoirs: AAPG Memoir 102, p. 137–152.

Salvador, A., 1987, Late Triassic-Jurassic paleogeography and origin of Gulf of Mexico Basin: AAPG Bulletin, v. 71, no. 4, p. 419–451.

Schieber, J., 1985, The relationship between basin evolution and genesis of stratiform sulfide horizons in mid-Proterozoic sediments of central Montana (Belt Supergroup): Dissertation, University of Oregon, Eugene, 811 p.

Schieber, J. 1998, Deposition of mudstones and shales: Overview, problems, and challenges, *in* J. Schieber, W. Zimmerle, and P. Sethi, eds., Shales and mudstones (vol. 1): Basin studies, sedimentology and paleontology: Stuttgart, Schweizerbart'sche Verlagsbuchhandlung, p. 131–146.

Schieber, J., 1999, Distribution and deposition of mudstone facies in the Upper Devonian Sonyea Group of New York: Journal of Sedimentary Research, v. 69, p. 909–925.

Schieber, J., 2003, Simple gifts and hidden treasures—Implications of finding bioturbation and erosion surfaces in black shales: The Sedimentary Record, v. 1, p. 4–8.

Schieber, J., J. B. Southard, and K. G. Thaisen, 2007, Accretion of mudstone beds from migrating floccule ripples: Science, v. 318, December 14, 2007, p. 1760–1763.

Schieber, J., and J. B. Southard, 2009, Bedload transport of mud by Floccule Ripples—Direct observation of ripple migration processes and their implications: Geology, v. 37, p. 483–486.

Schieber, J., and Z. Yawar, 2009, A new twist on mud deposition—Mud ripples in experiment and rock record: The Sedimentary Record, v. 7/2, p. 4–8.

Schieber, J., 2010, Common themes in the formation and preservation of intrinsic porosity in shales and mudstones—Illustrated with examples across the phanerozoic: n. 132370-MS, SPE Unconventional Gas Conference, February 23–25, 2010, Pittsburgh, Pennsylvania, USA.

Schieber, J., O. R. Lazar, M. K. Bohacs, R. Klimentidis, J. Ottmann, and M. Dumitrescu, 2012, A scanning electron microscope study of porosity in the Eagle Ford Shale of Texas: AAPG Search and Discovery Article #90142, AAPG Annual Convention and Exhibition, Long Beach, California.

Schieber, J., 2013, SEM observations on Ion-milled samples of devonian Black Shales from Indiana and New York: The petrographic context of multiple pore types, *in* W. Camp, E. Diaz, and B. Wawak, eds., Electron microscopy of shale hydrocarbon reservoirs: AAPG Memoir 102, p. 153–172.

Schieber, J., 2014, Traces in the dark—Sedimentary processes and facies gradients in the Upper Devonian–Lower Mississippian upper shale member of the Bakken Formation, Williston Basin, North Dakota, USA—Discussion. Journal of Sedimentary Research, v. 84, p. 837–838.

Surdam, R. C., D. B. MacGowan, and T. L. Dunn, 1991, Predictive models for sandstone diagenesis: Organic Geochemistry, v. 17, p. 243–253.

Syvitski, J. P. M., 1991, The changing microfabric of suspended particulate matter—The fluvial to marine transition: Flocculation, agglomeration, and pelletization, *in* R. H. Bennett, W. R. Bryant, and M. H. Hulbert, eds., Microstructure of fine-grained sediments: New York, Springer Verlag, p. 131–138.

Trevino, R. H., 1988, Facies and depositional environments of the Boquillas Formation, Upper Cretaceous of southwest Texas: M.S. Thesis, University of Texas, 135 p.